These results disclaim an asynchronous stepwise mechanism as predicted from the MINDO/3 calculations. In the present study the exploration of the relevant sections of the 4-21G hypersurface and the experimentally based information of the TS properties suggest that the MINDO/3 profile might be a numerical artifact.[67]

The STO-3G model produces poor descriptions of reaction profiles of the S_N2[68] and hydride exchange reactions.[50] In the present case, and in spite of the presence of a cationic species all along the pathway, the STO-3G model is again unsatisfactory. Therefore, STO-3G ME profiles for predicting the nature of the species along a reaction must be taken with circumspection.

The Meyer–Schuster rearrangement is a solvent-assisted reaction. The MSM is a first step toward representing solvent effects in the supermolecule approach. Even at this simple level the global hypersurface hints some of the roles passive many-body solvent effects might have on this reaction. Metropolis Monte Carlo simulations of hydration effects on the stationary points of the present reaction[7] have shown interesting solvation patterns. Solvent caging effects may play an important role in stabilizing the reactant and product of the RLS. Furthermore, if the solvation shell around the TS is allowed to equilibrate, the sample analysis shows the presence of two water molecules interacting with the C_2 center.[7] As we have seen before, increment in the number of water molecules has produced a change in the structure of the TS. The question arises, naturally, as to what may happen to the TS structure if another water molecule is added to the MSM and the system is treated as a new supermolecule. The present results obtained with the MSM are in fairly good agreement with available physical organic chemistry information. Therefore, one would not expect a departure from the simple molecular model used here.[46]

Acknowledgment. The computations have demanded huge amounts of CPU time over the recent years. We are most grateful to Uppsala Data Center for facilities made available in the CYBER 170-835 and IBM-Sweden for extensive use of the 4361 computer thanks to a Study Contract with the Molecular Biology Department. We thank the Immunology Department at BMC for letting us use their MICRO VAX-II without constraints. J.A. acknowledges a post-doctoral fellowship (curso 84/85) from the Spanish Government (Ministerio de Educacion y Ciencia) to carry out this research at the Chemistry and Molecular Biology Department, BMC. O.T. acknowledges financial support from the Swedish Research Council.

(66) Houk, K. N.; Lin, Y. T.; Brown, F. K. *J. Am. Chem. Soc.* **1986**, *108*, 554.
(67) The geometrical parameters for the stationary points with the 4-21G basis set have been given in the captions for Figures 5 and 6. These data can be used to check semiempirical methods in this type of study.
(68) Kost, D.; Aviram, K. *J. Am. Chem. Soc.* **1986**, *108*, 2006.
(69) (a) Zielinski, T. J.; Breem, D. L.; Rein, R. *J. Am. Chem. Soc.* **1978**, *100*, 6266. (b) Klopman, G.; Andreozzi, P.; Hopfinger, A. J.; Kikuchi, O.; Dewar, M. J. S. *J. Am. Chem. Soc.* **1978**, *100*, 6267.
(70) (a) McIver, J. W., Jr.; Stanton, R. E. *J. Am. Chem. Soc.* **1972**, *94*, 8618. (b) Stanton, R. E.; McIver, J. W., Jr. *J. Am. Chem. Soc.* **1974**, *96*, 3632.
(71) (a) Murrell, J. N.; Laidler, K. J. *Trans. Faraday Soc.* **1968**, *64*, 371. (b) Murrell, J. N.; Pratt, G. L. *Trans. Faraday Soc.* **1970**, *66*, 1680. (c) Murrell, J. N. *J. Chem. Soc., Chem. Commun.* **1972**, 1044.

Two-Dimensional Double-Quantum NMR Spectroscopy of Isolated Spin $^3/_2$ Systems: ^{23}Na Examples†

William D. Rooney, Thomas M. Barbara, and Charles S. Springer, Jr.*

Contribution from the Department of Chemistry, State University of New York, Stony Brook, New York 11794-3400. *Received April 6, 1987*

Abstract: Of the four possible types of NMR spectral behavior for a system consisting of isolated quadrupolar $I = {}^3/_2$ nuclei, double-quantum coherence can be excited by multipulse techniques in three. Two-dimensional ^{23}Na NMR spectra have been obtained from samples exhibiting each of these three. These are the following: (a) single crystal (represented here by an oriented lyotropic liquid crystal), (b) powder pattern (represented by an unoriented lyotropic liquid crystal), and (c) homogeneous biexponential relaxation (represented by a sufficiently dense solution of reasonably globular macromolecules). The fourth type, for which double quantum coherence generation by pulsed NMR is unknown, is the extreme narrowed situation. The pulse sequence $(90_x\text{-}\tau/2\text{-}180_y\text{-}\tau/2\text{-}90_x\text{-}t_1\text{-}90_x\text{-}t_2)$ generates a two-dimensional spectrum when the response is sequentially Fourier transformed from the t_2 and t_1 time domains. The projection onto ν_2 is the single-quantum spectrum while the projection onto ν_1 is the double-quantum spectrum (given appropriate phase cycling of the pulse sequence). The double-quantum spectrum is quite distinct for all three spectral types. This is also true for the single-quantum spectrum. However, the latter is less diagnostic and is subject to distortions from an insufficiently short receiver dead time, while the former is not. In addition, all of the double-quantum spectral information derives from modulation of the strong, sharp central single-quantum signal. Thus, this experiment can be useful in cases where the broad satellite resonance(s) is (are) not detectable in the single-quantum spectrum because of electric field gradient effects on the quadrupolar nucleus. This is often the case in tissue-containing samples. The theory of this experiment is briefly discussed, as are the differing requirements for the excitation of double quantum coherence for type a and type b spectra on the one hand and type c spectra on the other. Drawbacks of this approach, particularly the trade-off between total acquisition time and digital resolution in the ν_1 dimension, are also considered.

In conventional single quantum (1Q) NMR spectroscopy and imaging, adjacent states established by the Zeeman interaction are brought into coherent superposition by the absorption or emission of a radio frequency photon. The 1Q NMR spectra of nuclei with electric quadrupole moments ($I \geq 1$, where I is the nuclear spin quantum number) are often strongly affected by interactions with electric field gradients (EFG). Potentially, these interactions contain a wealth of information about the system under study. Unfortunately, they are often difficult (sometimes impossible) to measure in the standard 1Q NMR experiment. Important examples of this arise in the ^{23}Na and ^{39}K (both $I = {}^3/_2$ nuclei) spectra from living systems.[1] These are isotopes of

† Presented in part, at the March Meeting of the American Physical Society, New York, NY, March, 18, 1987 (abstract: *Bull. Am. Phys. Soc.* **1987**, *32*, 644) and the 28th Experimental Nuclear Magnetic Resonance Spectroscopy Conference, Asilomar, CA, April, 5, 1987.

(1) Springer, C. S. *Annu. Rev. Biophys. Biophys. Chem.* **1987**, *16*, 375-399.

0002-7863/88/1510-0674$01.50/0

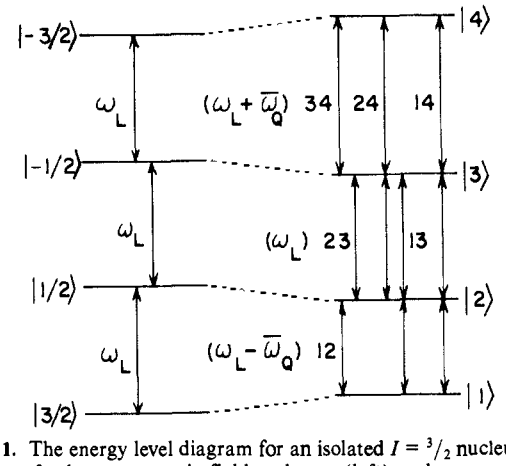

Figure 1. The energy level diagram for an isolated $I = {}^3/_2$ nucleus in the presence of a large magnetic field and zero (left) and nonzero (right) averaged electric field gradient magnitude-orientation products.

high natural abundance (100% and 93%, respectively) of elements that are ubiquitous in nature in both extent and amount. In fact, in repetitive pulse experiments, the ^{23}Na signal is the second strongest in biology, despite the fact that part of it is often not detectable in conventional spectra and images because of quadrupolar effects.

States differing by more than one nuclear spin magnetic quantum number can be brought into coherent superposition by suitable manipulation of the spin system. This is the realm of multiple quantum (MQ) NMR.[2-5] MQ NMR is often used as an aid in spectral interpretation. In general, the number of observed transitions decreases with increasing p-quantum excitation, leading to spectral simplification.[2]

In principle, the isolated, quadrupolar $I = {}^3/_2$ nucleus can undergo single (12, 23, and 34) (Figure 1), double (13 and 24), and triple (14) quantum NMR transitions. As understood now, the prerequisite for actual MQ excitation in pulsed spin $^3/_2$ NMR is that the nucleus be not at the extreme narrowing limit. That limit is defined as the situation when $\tau_c \ll \omega_L^{-1}$, where τ_c is the *longest* correlation time of the fluctuating EFG magnitude-orientation product at the nucleus and ω_L^{-1} is the inverse angular Larmor frequency. (In frequency units, the EFG-magnitude-orientation product for an axial EFG is $eq(4\hbar)^{-1}(3\cos^2\theta - 1)$, where eq is the major element of the EFG tensor, θ is the angle of the molecular axis of the EFG tensor with the Zeeman magnetic field direction, and e and $\hbar$ have their usual meanings. This is also equal to $\omega_Q(eQ)^{-1}$ in this paper, where eQ is the electric quadrupole moment of the nucleus. The quantities q and θ, and therefore ω_Q, are time dependent.) In very many of the spin $^3/_2$ systems of interest (e.g., ^{23}Na and ^{39}K), there is more than one correlation time. Very often, one or more of these is much smaller than ω_L^{-1}. Thus, for MQ excitation, at least one correlation time must be $\geq\omega_L^{-1}$. Even when this condition is satisfied, the nature of the spectrum, and also the mechanism of MQ excitation, depends on the order of the environment and the actual magnitude of τ_c.

In an ordered environment where the axes of the EFG tensors assume only one (or a limited range of) orientation with respect to the magnetic field, the 1Q spectrum consists of a sharp central component (23, Figure 1), representing 40% of the total signal intensity, flanked by two broader components (12 and 34, Figure 1) accounting for 30% of the total signal intensity each a single crystal-type spectrum. If there are *also* short correlation times, which are $\ll(\omega_Q^0)^{-1}$, where ω_Q^0 is the limiting angular quadrupolar frequency, the EFG magnitude-orientation product may be partially averaged, but a single crystal-type spectrum is still manifest. This is why the time-averaged value of $\omega_Q(t)$, $\bar{\omega}_Q$ ($\neq 0$), appears in Figure 1. This can be the case in samples consisting of oriented liquid crystalline domains or oriented biopolymers.

Unoriented, macroscopically isotropic samples are, however, much more common. In this case, the effective EFG axes have random orientations with respect to the magnetic field. It is here that the nature of the spectrum and the mechanism of MQ excitation must be carefully distinguished. There are two extremes. When $\tau_c \gg \bar{\omega}_Q^{-1}$, a 1Q spectrum is obtained which is the superposition of the 23 singlet and many 12, 34 doublets—an inhomogeneous "powder pattern". The other extreme occurs when $\tau_c \ll \bar{\omega}_Q^{-1}$ (but still $\geq\omega_L^{-1}$). In this case, both longitudinal and transverse relaxation exhibit biexponential behavior. The resulting 1Q spectrum is the superposition of broad (60%, 12 and 34, Figure 1) and narrow (40%, 23, Figure 1) lines at the same frequency. Hence, in this extreme, the effective value of $\bar{\omega}_Q$ is zero. This is the homogeneous biexponential quadrupolar spectrum.[1]

Thus, there are four types of spectrum possible for isolated spin $^3/_2$ containing samples: (a) single crystal-like, (b) inhomogeneous powder pattern, (c) homogeneous biexponential, and (d) extreme narrowed. It has long been known that for type a and b spectra of isolated $I = 1$ systems, MQ coherence (MQC) can be created because of the residual quadrupolar splittings (e.g., ref 6). It has been only more recently realized that MQC can also be created in type c spectra (which are not possible for isolated spin 1 systems) due to the multiexponential character of the relaxation.[7-11]

A problem often encountered in 1Q ^{23}Na (and ^{39}K) NMR studies of biological tissue is a signal intensity lower than that expected from the amount of Na^+ (or K^+) known to be present; the phenomenon of "NMR invisibility". Almost certainly this is due to the interaction between the quadrupolar nucleus and the much varied EFG magnitude-orientation products the nucleus encounters in biological tissue, which does not comprise a totally oriented sample. Depending on the value of τ_c, the broad component(s) may become unobservable in spectra ranging from pure type b to pure type c, leading to signal intensity losses of up to 60%.[1,12-14] In extreme cases of type b, signal intensity losses of up to 80% could be anticipated.[15-19]

Joseph and Summers have recently suggested that measurement of the nutation frequency of the 1Q central line (23, in Figure 1) can be used to distinguish between the type b and type c mechanistic extremes giving rise to NMR invisibility.[20] In this paper, we will show that the nature of the double quantum (2Q) spectrum can also be very diagnostic of the mechanistic details of the interactions giving rise to NMR invisibility in the 1Q spectrum. The 2Q experiment may offer advantages over the nutation experiment in that the latter has stringent hardware requirements and may be less diagnostic. However, the 2Q experiment can be quite time-consuming.

Theory

In this section we briefly describe the methods and efficiency of generating 2Q coherence (2QC) for isolated spin $^3/_2$ nuclei.

(2) Munowitz, M.; Pines, A. *Science* **1986**, *233*, 525-531.
(3) Drobny, G. P. *Annu. Rev. Phys. Chem.* **1985**, *36*, 451-489.
(4) Weitekamp, D. P. *Adv. Magn. Reson.* **1983**, *11*, 111-274.
(5) Bodenhausen, G. *Prog. NMR Spectrosc.* **1981**, *14*, 137-173.
(6) Miner, V. W.; Tyrell, P. M.; Prestegard, J. H. *J. Magn. Reson.* **1983**, *55*, 438-452.
(7) Müller, N.; Bodenhausen, G.; Wüthrich, K.; Ernst, R. R. *J. Magn. Reson.* **1985**, *65*, 531-534.
(8) Rance, M.; Wright, P. E. *Chem. Phys. Lett.* **1986**, *124*, 572-575.
(9) Pekar, J.; Leigh, J. S. *J. Magn. Reson.* **1986**, *69*, 582-584.
(10) Pekar, J.; Renshaw, P. F.; Leigh, J. S. *J. Magn. Reson.* **1987**, *72*, 159-161.
(11) Jaccard, G.; Wimperis, S.; Bodenhausen, G. *J. Chem. Phys.* **1986**, *85*, 6282-6293.
(12) Berendsen, H. J. C.; Edzes, H. T. *Ann. NY Acad. Sci.* **1973**, *204*, 459-485.
(13) Shporer, M.; Civan, M. *Curr. Top. Membr. Transp.* **1977**, *9*, 1-69.
(14) Forsén, S.; Lindman, B. *Methods Biochem. Anal.* **1981**, *27*, 289-486.
(15) Schmidt, V. H. *Pulsed Magnetic and Optical Resonance* **Blinc**, R., Ed.; J. Stefan Institute: Ljubljana, Yugoslavia, 1971; pp 75-83.
(16) Samoson, A.; Lippmaa, E. *Chem. Phys. Lett.* **1983**, *100*, 205-208.
(17) Fenzke, D.; Freude, D.; Fröhlich, T.; Haase, J. *Chem. Phys. Lett.* **1984**, *111*, 171-175.
(18) Pandey, L.; Towta, S.; Hughes, D. G. *J. Chem. Phys.* **1986**, *85*, 6923-6927.
(19) Kentgens, A. P. M.; Lemmens, J. J. M.; Geurts, F. M. M.; Veeman, W. J. *J. Magn. Reson.* **1987**, *71*, 62-74.
(20) Joseph, P. M.; Summers, R. M. *Mag. Res. Med.* **1987**, *4*, 67-77.

We take the rotating frame Hamiltonian to be that given in eq 1, where δ is the resonance offset and the other operator symbols have their usual meanings.

$$\mathcal{H} = -\delta I_z + (\bar{\omega}_Q/6)\{3I_z^2 - \mathbf{I}\cdot\mathbf{I}\} \quad (1)$$

In the extreme where motion does not average $\bar{\omega}_Q$ to zero (types a and b), there are a number of possible MQ experiments. The creation of MQC for $I = {}^3/_2$ with the use of selective pulse techniques has been discussed by Vega[21,22] and Ernst.[23] Alternatively, two- and three-quantum coherence should be achievable, in the usual fashion,[3-5] with a pair of sufficiently hard 90° pulses separated by a period of free precession. To the best of our knowledge, however, the description of 2QC generation by a pair of strong RF pulses (though well presented for spin 1 (e.g., ref 6, 24, and 25)) has not previously been reported for $I = {}^3/_2$. In the extreme where $\bar{\omega}_Q$ is averaged to zero by motion (type c), the creation of MQC via biexponential relaxation has been reported by Pekar and Leigh[9] and thoroughly discussed by Bodenhausen and co-workers.[11]

In either case, calculations are easily carried out with an operator expansion in a basis of irreducible tensor operators.[26] Many of the necessary formulae for spin $^3/_2$ have been conveniently tabulated by Bowden et al.[27] A detailed discussion of the spin system's evolution during the pulse sequence given in Figure 2a will not be given here. Only the observable magnetization after 2Q filtering (i.e., after the τ and t_1 periods of Figure 2a and appropriate phase cycling) is presented.

For the extreme when $\bar{\omega}_Q \neq 0$, the effects of relaxation can be ignored for the moment, and for zero offset excitation (i.e., $\delta = 0$) in the absence of finite pulse width effects, we find that the transverse magnetization observable during t_2 is given by eq 2

$$\langle I_y(t_1,t_2)\rangle = A(\bar{\omega}_Q,\tau)\{2\cos(\bar{\omega}_Q t_1 - \phi)\sin\bar{\omega}_Q t_2 - \sin(\bar{\omega}_Q t_1 - \phi)\cos\bar{\omega}_Q t_2 - \sin(\bar{\omega}_Q t_1 - \phi)\} \quad (2)$$

where

$$A(\bar{\omega}_Q,\tau) = ({}^3/_2)\sin\bar{\omega}_Q(\tau/2)(\sin^2\bar{\omega}_Q(\tau/2) + 4\cos^2\bar{\omega}_Q(\tau/2))^{1/2} \quad (3)$$

and

$$\tan\phi = ({}^1/_2)\tan\bar{\omega}_Q(\tau/2) \quad (4)$$

Equation 2 shows that during t_1, the central transition (third term on RHS) is modulated in amplitude (at $\bar{\omega}_Q$), whereas the satellite transitions (a linear combination of the first two terms on RHS) are modulated in phase as well. The essential distinction between an isolated spin $^3/_2$ and the more familiar case of two coupled spin $^1/_2$ nuclei is the following. In the former, free precession under $\mathcal{H}$ (during τ) will produce antiphase 1Q coherences of rank three and rank two,[27] the intensities of which oscillate, while, in the latter case, there is only rank two coherence. Double quantum coherences of both ranks can therefore be produced by the second 90_x pulse in the spin $^3/_2$ case and, during t_1, these oscillate in intensity as they each precess at $\bar{\omega}_Q$. As a result, the overall efficiency of 2Q generation, given by $A(\bar{\omega}_Q,\tau)$, is less sensitive to a particular choice of τ (illustrated in Figure 2b) than is the case for two coupled spin $^1/_2$ nuclei where the excitation peaks, though occurring at the same intervals, are narrower. This feature is a distinct advantage when one desires to produce 2QC over the wide range of $\bar{\omega}_Q$ values present in inhomogeneously broadened powder patterns (type b).

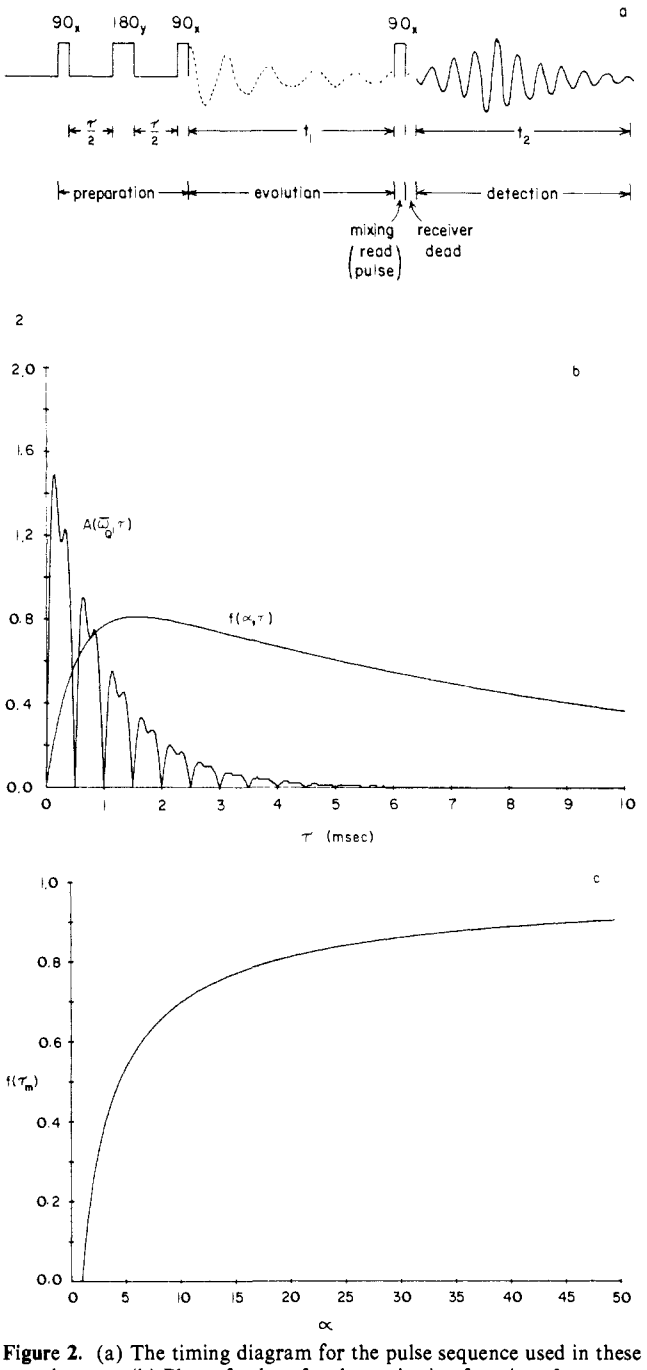

Figure 2. (a) The timing diagram for the pulse sequence used in these experiments. (b) Plots of values for the excitation functions for generating double quantum coherence for spin $^3/_2$ systems exhibiting type a (or b) and type c spectral behavior. For $A(\bar{\omega}_Q,\tau)$, $\bar{\omega}_Q/2\pi$ is held equal to 1 kHz and R for the 2nd and 3rd rank 1QC is 10^3 s^{-1} for each. For $f(\alpha,\tau)$, α is held equal to 20 and R^{1Q} is 100 s^{-1}. See the text for details. (c) The maximum value of the excitation function for double quantum coherence, for the spin $^3/_2$ system exhibiting type c spectral behavior, as a function of α. See the text for details.

We give, for completeness, the transverse relaxation rate constants in the case of nonzero $\bar{\omega}_Q$ much larger than the homogeneous line widths. We obtain (from Redfield theory) eq 5

$$R_s^{1Q} = 6C^2(J_1(\omega_L) + J_2(2\omega_L)) \quad (5a)$$

$$R_f^{1Q} = 6C^2(J_0(0) + J_1(\omega_L) + J_2(2\omega_L)) \quad (5b)$$

$$R^{2Q} = 6C^2(J_0(0) + J_1(\omega_L) + J_2(2\omega_L)) \quad (5c)$$

where R_s^{1Q}, R_f^{1Q}, and R^{2Q} are the rate constants for the slow and fast 1Q components and the 2QC, respectively. The $J_q(q\omega_L)$ denote, as usual, the spectral densities of the motion of the fluctuating EFG magnitude-oreintation products and the constant C is equal to $eQ/6\hbar$ ($\hbar$ has its usual meaning).

(21) Vega, S.; Naor, Y. *J. Chem. Phys.* **1981**, *75*, 75-86.
(22) Vega, S. *J. Chem. Phys.* **1978**, *68*, 5518-5527.
(23) Wokaun, A.; Ernst, R. R. *J. Chem. Phys.* **1977**, *67*, 1752-1758.
(24) Vega, S.; Pines, A. *J. Chem. Phys.* **1977**, *66*, 5624-5644.
(25) Bodenhausen, G.; Vold, R. L.; Vold, R. R. *J. Magn. Reson.* **1980**, *37*, 93-106.
(26) Corio, P. L. *J. Math. Phys.* **1968**, *9*, 1067-1071.
(27) Bowden, G. J.; Hutchinson, W. D.; Khachan, J. *J. Magn. Reson.* **1986**, *67*, 415-437.

In the extreme when the effective value of $\bar{\omega}_Q = 0$ (type c), relaxation effects must be explicitly taken into consideration. For excitation with an offset δ, the observable magnetization is given by eq 6. Similar equations have been reported.[9,11] The factor

$$\langle I_y(t_1,t_2)\rangle + i\langle I_x(t_1,t_2)\rangle = (^3/_4)f(\tau)f(t_2)e^{-R^{2Q}t_1}\cos 2\delta t_1 e^{i\delta t_2} \quad (6)$$

$f(\tau)$, the efficiency of generating 2QC, is given in eq 7 and, in terms of α, ($\alpha = R_f^{1Q}/R_s^{1Q}$), in eq 8. (See Figure 2b.) For a

$$f(\tau) = e^{-R_s^{1Q}\tau} - e^{-R_f^{1Q}\tau} \quad (7)$$

$$f(\alpha,R_s^{1Q},\tau) = f(\alpha,\tau) = e^{-R_s^{1Q}\tau} - (e^{-R_s^{1Q}\tau})^\alpha \quad (8)$$

given value of α, the generation of 2QC is a maximum for a creation period, τ_m, given by equation 9

$$\tau_m = \frac{1}{R_s^{1Q}}\left\{\frac{\ln \alpha}{\alpha - 1}\right\} \quad (9)$$

and

$$(f(\tau))_{max} = f(\tau_m) = \alpha^{-\alpha/(\alpha-1)} - \alpha^{-1/(\alpha-1)} \quad (10)$$

From eq 10, one can see that the efficiency of generating 2QC approaches unity only in the limit of $\alpha \gg 1$ and can be quite small for nearly equal fast and slow 1Q transverse relaxation rate constants. (A very similar result has also been calculated by Pekar (J. Pekar, private communication).) The maximum amplitude of 2QC generation as a function of α is shown in Figure 2c. Moreover, the overall strength of the 2Q filtered signal is proportional to the product $f(\tau)f(t_2)$ since the transfer of 2QC back into observable magnetization involves the reverse of the creation process. The function $f(t_2)$ is given in eq 11. This places strong demands on sensitivity. For example, at $\alpha = 2$, the 2Q filtered

$$f(t_2) = e^{-R_s^{1Q}t_2} - e^{-R_f^{1Q}t_2} \quad (11)$$

signal is roughly $^1/_{20}$ as strong as that obtained from the free induction decay resulting from a single 90° pulse.

The explicit expressions for R_s^{1Q}, R_f^{1Q}, and R^{2Q} in the case where the effective value of $\bar{\omega}_Q$ is zero are given in eq 12. If the motion of the nucleus can be described by a single value for τ_c,

$$R_s^{1Q} = 6C^2(J_1(\omega_L) + J_2(2\omega_L)) \quad (12a)$$

$$R_f^{1Q} = 6C^2(J_0(0) + J_1(\omega_L)) \quad (12b)$$

$$R^{2Q} = 6C^2(J_0(0) + J_2(2\omega_L)) \quad (12c)$$

we can expect $R_s^{1Q} < R^{2Q} < R_f^{1Q}$ away from the extreme narrowing limit. Although R^{2Q} and R_f^{1Q} are equally sensitive to slow motion, via $J_0(0)$, J_0 can be more easily determined with the double quantum experiment which does not suffer from dead time problems during t_1. In contrast to the case of nonzero $\bar{\omega}_Q$, only rank three 2QC is generated in this case. Equation 12c corrects an error in the report of Jaccard et al.[11] in assigning R^{2Q} to the decay of the unobservable rank two 2QC (G. Bodenhausen, private communication). It is quite interesting to note that in this case the rate constant for the 1Q satellites (eq 12b) is not the same as that for the 2Q line (eq 12c). This is in contrast to the type b spectrum (eq 5). The central transition has the same rate constant in each case (eq 5a and 12a).

Experimental Section

1. Preparation of Nematic Lyotropic Phases. Mesophases consisting of approximately equal weight percentages of sodium detergents and water can give rise to first-order quadrupolar splitting in ^{23}Na NMR.[28] If viscous forces are small compared to the torque created by the interaction of the static magnetic field and the diamagnetic anisotropy of the phase, the liquid crystalline domains in the sample can become oriented with respect to the field.[28,29] The orientation in the sample increases with time in the magnetic field, and a single crystalline spectral behavior (type a) is asymptotically approached.

Sample A. A ternary mesophase was chosen[30] that gave rise to moderate residual quadrupolar splitting ($\bar{\omega}_Q/2\pi$ equal to 17.0 kHz). The weight percent composition of the mesophase was 37% (w/w) sodium dodecylsulfate (Sigma Chemical Co.), 11% *n*-decyl alcohol (Sigma), and 52% deuterium oxide (Cambridge Isotope Laboratories). This mesophase, being type I CM (cylindrical micellar),[28] gave rise to a sample that, after 3–4 months of aging, with repeated exposures to the magnetic field, could be quite well ordered.

Sample B. A slightly different ternary mesophase consisting of 38% sodium dodecylsulfate, 12% *n*-decyl alcohol, and 50% deuterium oxide[30] was also prepared. At ca. 20 °C, the ^{23}Na NMR spectrum of this mesophase, also type I CM, was an inhomogeneous quadrupolar powder pattern (type b) when it was obtained shortly after sample placement in the magnet. Also, this sample was used when it was relatively fresh (only ca. one month old) and had suffered fewer exposures to the magnetic field.

2. Preparation of Serum Albumin Solution. Sample C. Five grams of bovine serum albumin (Sigma) was dissolved in 10.0 mL of deuterium oxide containing 1.5 g of NaCl. This sample gives rise to a homogeneous biexponentially relaxed quadrupolar spectrum (type c).[9]

3. NMR Spectroscopy. A Nicolet NT-300 NMR spectrometer (7.05 T) operating at the ^{23}Na resonant frequency of 79.38 MHz was used for all experiments. The pulse sequence employed was that shown in Figure 2a. The phases of the RF pulses produced by the pulse programmer were calibrated, prior to the experiments, using the procedure described by Habenreisser and Schnabel.[31] The 180° pulse (35.0 μs) sandwiched between the first and second 90° pulses (17.5 μs) achieves independence from any resonant offset, δ (shift), during the 2Q creation period (τ). The values of τ employed ranged from microseconds to milliseconds depending on the sample (see Theory section). The 2Q evolution occurs during the t_1 time domain. The spectral width and digital resolution in the ν_1 dimension are given by eq 13 and 14

$$SW(\nu_1) = \pm (2DW)^{-1} \quad (13)$$

$$DR(\nu_1) = (nDW)^{-1} \quad (14)$$

where DW is the time increment of t_1, and n is the total number of data points collected in t_1 (i.e., the number of t_1 values). Both $SW(\nu_1)$ and $DR(\nu_1)$ were adjusted according to sample requirements, and the latter is given for each experiment in the figure legend. (In general, $SW(\nu_1)$ should be set equal to $SW(\nu_2)$.) In order to reduce coherent noise and unwanted signals (particularly 1QC) from the final spectrum, a 32-step phase cycle routine, which is described in the literature,[32] was used. This cycle selects for the even pQC: $p = 2, 6, 10$, etc. Since there are no even coherences with $p > 2$ in this system, this is a quite effective 2Q-pass filter. Thus, for given values of τ and t_1, the number of free induction decays accumulated was an integral multiple of 32. (For the spectra in Figures 3, 4, and 5, the integers were 8, 16, and 8, respectively.) Data processing was performed on a Nicolet/GE 1280 data station. The processing employed produced absolute value spectra. The 2D spectral projections were those of the standard GE 2DNMR software. Those shown in this paper are the digital summations of all frequency elements perpendicular to the display axes. The integrations were achieved with use of the GE GENCAP curve-resolution subroutine.

Results

In order to obtain a good example of a single crystal-type spectrum (type a), the well-aged liquid crystalline sample A was placed in the spectrometer magnet (7.05 T) for 6 h at 22 °C. After this period of time, the liquid crystalline domains, which are probably of the hexagonal form,[28] are well aligned parallel to each other. The two-dimensional 2Q (2D2Q) spectrum shown in Figure 3 results after a subsequent 2.1 h of signal acquisition. Figure 3a shows the stacked plot version of the spectrum in which the horizontal axis is ν_2 and the oblique axis is ν_1. Rows of small t_1 noise peaks, running parallel to ν_1, are evident as are two small cross peaks correlating the two satellite transitions. Figure 3b depicts a contour plot view of this spectrum. Projections c and d of Figure 3 are the projections of the spectrum on the ν_2 and ν_1 axes, respectively. The projection onto ν_2 (Figure 3c) is clearly the 1Q spectrum (three lines: relative intensities 0.31:0.40:0.30; total splitting, $2\bar{\omega}_Q/2\pi = 33.9$ kHz) and the projection onto ν_1 (Figure 3d) is clearly the 2Q spectrum (two lines: relative intensities 0.52:0.48; splitting = 33.8 kHz). It is analogous to the 1Q spectrum of an oriented isolated $I = 1$ system. The 1Q and 2Q spectra (figure 3, c and d) indicate that rather good alignment

(28) Forrest, B. J.; Reeves, L. W. *Chem. Rev.* **1981**, *81*, 1–14.
(29) Lawson, K. D.; Flautt, T. J. *J. Am. Chem. Soc.* **1967**, *89*, 5489–5491.
(30) Radley, K.; Reeves, L. W.; Tracey, A. S. *J. Phys. Chem.* **1976**, *80*, 174–182.
(31) Habenreisser, U.; Schnabel, B. *J. Magn. Reson.* **1979**, *35*, 175–184.
(32) Bax, A.; Freeman, R.; Kempsell, S. P. *J. Am. Chem. Soc.* **1980**, *102*, 4849–4851.

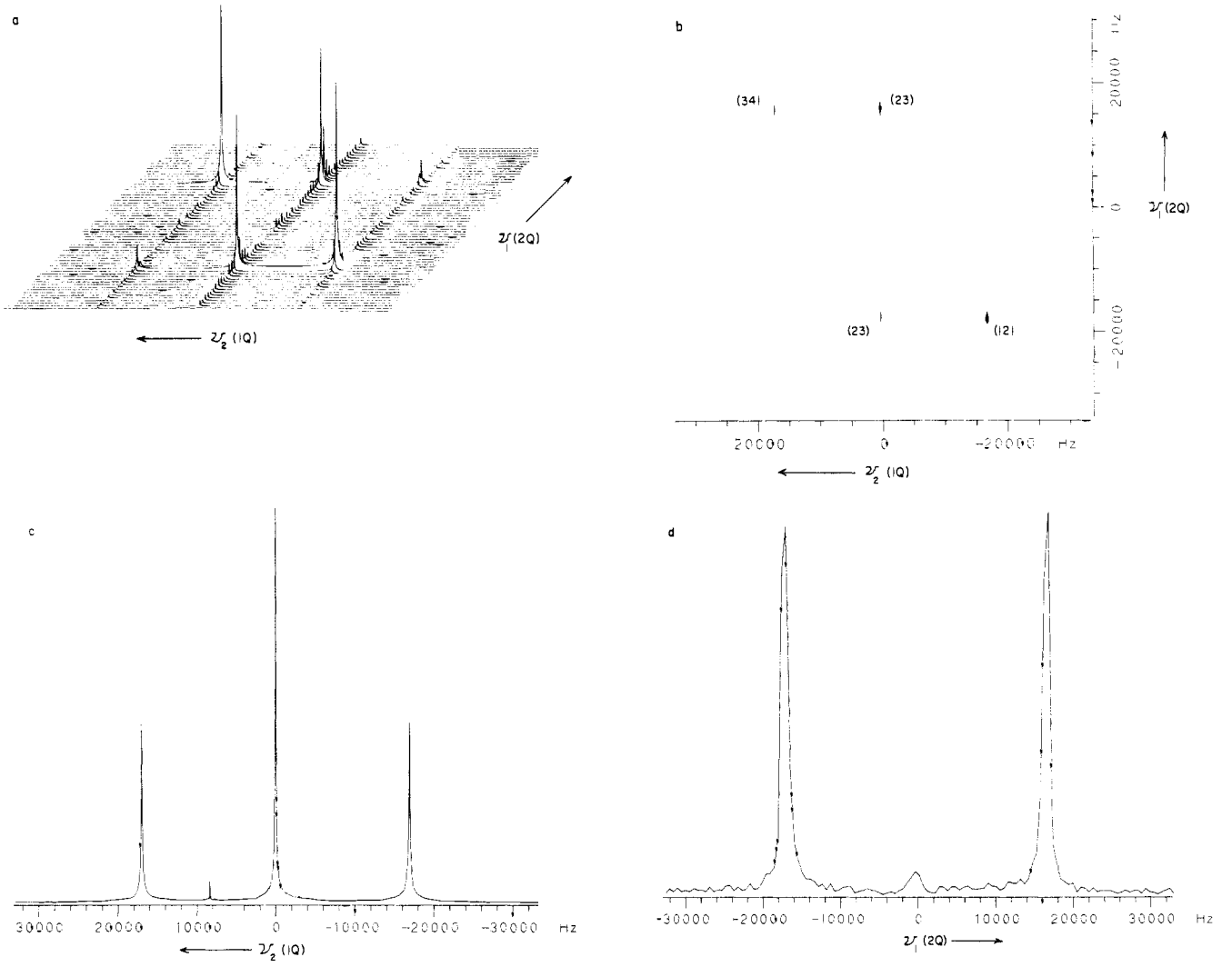

Figure 3. (a) The stacked plot of a two-dimensional double-quantum ^{23}Na NMR spectrum of an oriented liquid crystal (sample A). The value of τ was 20 μs. For t_1, 128 (n) increments of 15 μs (DW) each were used to vary t_1 from 15 μs to 1.92 ms. Thus, DR(ν_1) = 521 Hz. The effective receiver dead time after the last 90° pulse was 25 μs. The final value of t_2 was 30.72 ms and an additional 200 ms was inserted at the end of every t_2 period. Since eight 32-step phase cycles were employed, the total time was 2.1 h. (In the plot depicted, only 64 of the ν_1 increments are shown.) (b) A contour plot of the spectrum in part a. (c) The projection of the spectrum of part a onto the ν_2 axis. (d) The projection of the spectrum of part a onto the ν_1 axis.

was indeed achieved. The fact that the observed total splitting, ca. 34 kHz, is small compared to the MHz splittings which can be seen in true single crystals[33] suggests that there is a great deal of averaging occurring. The relative line widths of the central transition (65.6 ± 1.7 Hz) and the satellite transitions (128.3 ± 2.9 and 114.1 ± 2.3 Hz) should be noted, even though the latter may suffer from any residual sample inhomogeneities resulting from imperfect alignment of the domains. In addition to the effects of imperfect domain alignment and increased sensitivity to field inhomogeneities, the poor digital resolution of the 2Q spectrum (Figure 3d) also hinders an accurate estimation of the true line widths there (measured to be 654 ± 14 and 451 ± 6 Hz). These should be the same as those of the 1Q satellite peaks (eq 5b and 5c). Unfortunately, doubling the digital resolution (decreasing DR(ν_1) by a factor of 2) requires increasing the time of the experiment by a factor of 2 (eq 14).

If the liquid crystalline domains have totally random alignments, an axial powder pattern (type b) results. (The EFG tensor sensed by the Na^+ ion has axial symmetry.) Figure 4 shows a good example of a 2D2Q powder pattern spectrum. It was obtained from the less aged sample B which was in the magnet for only 2.0 h (the total time for spectral acquisition) at ca. 20 °C. The liquid-crystalline domains of sample B are probably also of the hexagonal form.[28] Figure 4a is the stacked plot; 4b, a contour plot; and 4c and 4e, the projections onto the ν_2 and ν_1 axes, respectively. Figure 4d depicts an expansion of the vertical scale of Figure 4c (the latter has the value required to display the entire central transition). The tops of some of the t_1 noise spikes evident in parts a, b, and c of Figure 4, are deleted in Figure 4d. The powder pattern of the satellite transitions is much more evident in part d than c of Figure 4. In fact, the parallel edges at ± ca. 19 kHz are almost impossible to discern in Figure 4c. As is expected for type I CM systems,[28] comparison with Figure 4 indicates that the alignment giving rise to the spectrum in Figure 3 was that with the Na^+-containing domains oriented with their cylindrical axes parallel to the magnetic field direction. The 2Q spectrum seen in Figure 4e is, of course, also an axial powder pattern.

The third kind of spectrum for which 2Q coherence can be excited by pulse techniques is that of homogeneous biexponential relaxation (type c). An example of this is the 2D2Q spectrum of sample C, obtained with 3.0 h of acquisition at ca. 20 °C, shown in Figure 5. Figure 5a is the stacked plot, 5b, a contour plot, and 5c and 5d, the projections onto ν_2 and ν_1, respectively. In this case, the 1Q spectrum projected onto ν_2 should be the superposition of two Lorentzian functions and can be well simulated with two of line widths 43.4 and 124.2 Hz and relative intensities of 50% each (inset of Figure 5c). (Strictly speaking, the peaks in absolute

(33) Derbyshire, W.; Stuart, J. P. *Magnetic Resonance and Radiofrequency Spectroscopy*; Averbuch, P., Ed.; Elsevier/North-Holland: Amsterdam, 1969; pp 403–408.

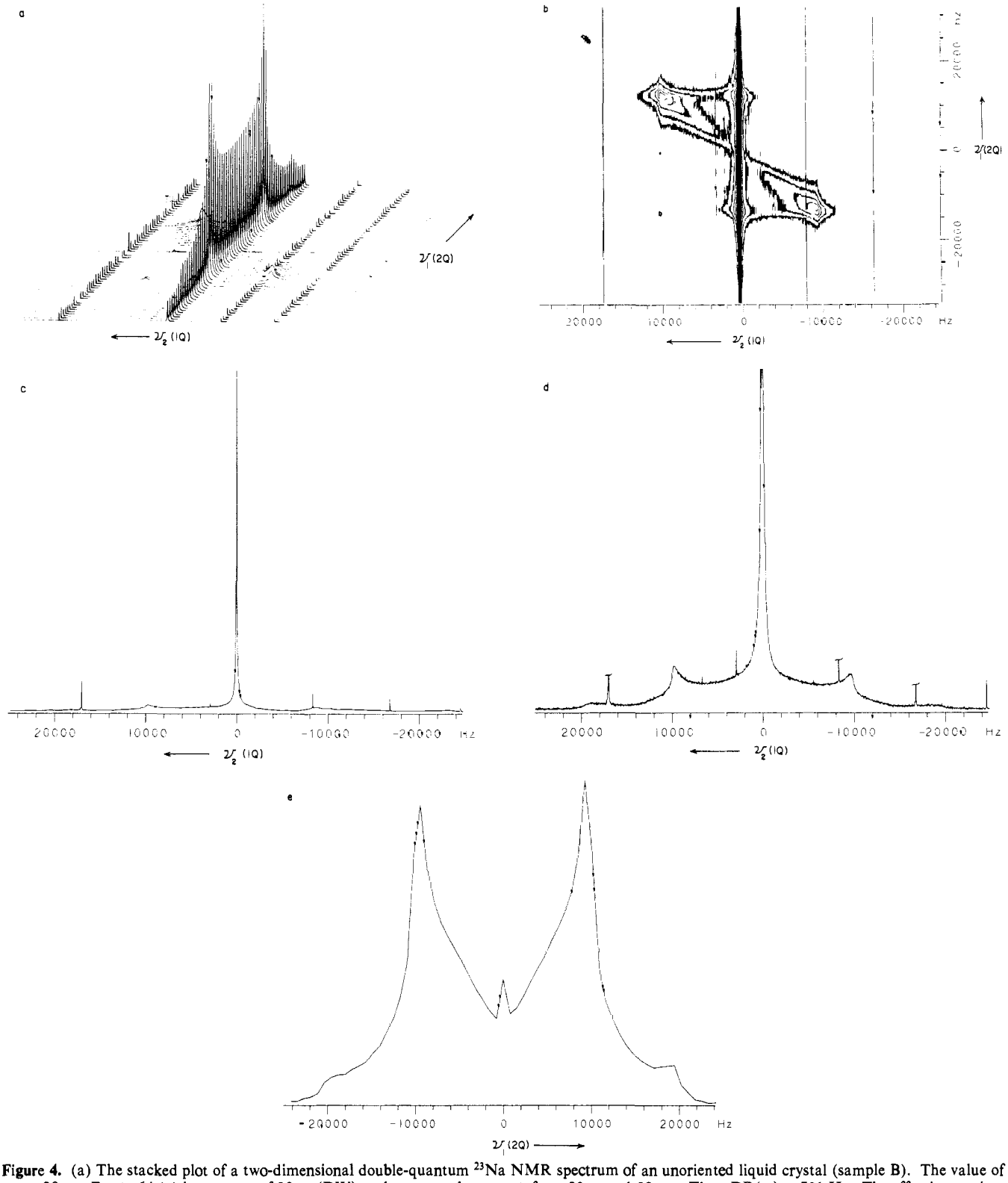

Figure 4. (a) The stacked plot of a two-dimensional double-quantum ^{23}Na NMR spectrum of an unoriented liquid crystal (sample B). The value of τ was 20 μs. For t_1, 64 (n) increments of 20 μs (DW) each were used to vary t_1 from 20 μs to 1.28 ms. Thus, DR(ν_1) = 781 Hz. The effective receiver dead time after the last 90° pulse was 30 μs. The final value of t_2 was 40.96 ms and an additional 200 ms was inserted at the end of every t_2 period. Since 16 32-step phase cycles were employed, the total time was 2.0 h. (b) A contour plot of the spectrum in part a. (c) The projection of the spectrum of part a onto the ν_2 axis. (d) The same as part c but with an expanded vertical scale. (e) The projection of the spectrum of part a onto the ν_1 axis.

value spectra do not have Lorentzian shapes. Also, a 10-Hz line-broadening sensitivity enhancement was applied.)

One could use these line widths to obtain values for R_s^{1Q} and R_f^{1Q}. However, Pekar and Leigh have suggested a more accurate way of measuring these quantities. This is a pseudo-2D experiment where the intensity of the 2Q-filtered 1Q signal ($f(\tau)$, in eq 7) is monitored (after a fixed value of t_1) as a function of the creation time, τ. The resulting excitation function (Figure 2b) can be fitted with R_s^{1Q} and R_f^{1Q} as parameters.[9] Although this experiment is usually not as lengthy as the 2D2Q experiment reported here, it is still quite time-consuming.

In contrast to the type a and type b cases above, the 2Q spectrum projected onto ν_1 should be a single Lorentzian (absolute value, here) peak and can be simulated with one of line width 246.6 Hz (inset of Figure 5d). The poor digital resolution of the 2Q spectrum, DR(ν_1), as well as the increased sensitivity to field

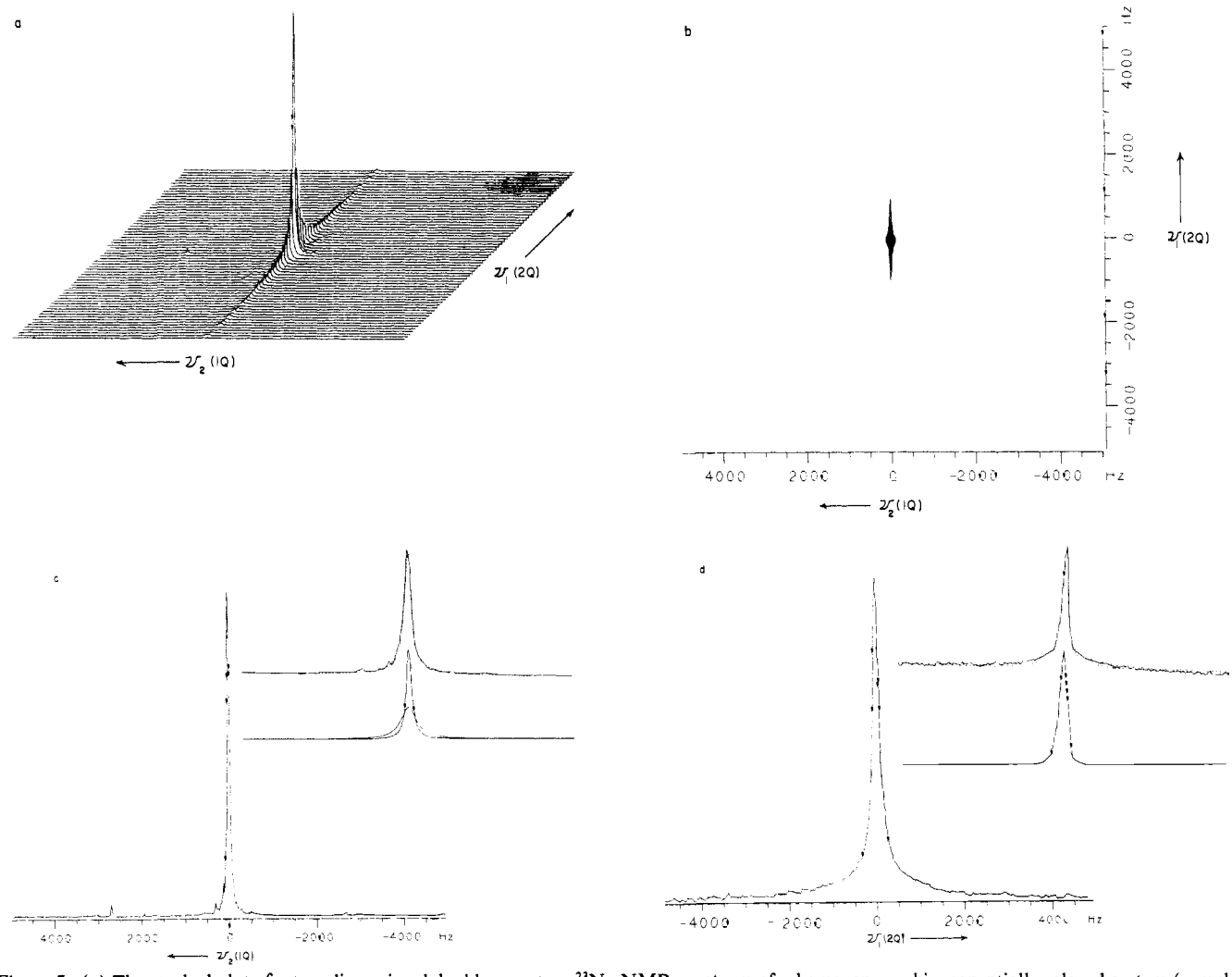

Figure 5. (a) The stacked plot of a two-dimensional double-quantum ^{23}Na NMR spectrum of a homogeneous biexponentially relaxed system (sample C). The value of τ was 3.4 ms. For t_1, 128 (n) increments of 100 μs (DW) each were used to vary t_1 from 100 μs to 12.8 ms. Thus, DR(ν_1) = 78 Hz. The effective receiver dead time after the last 90° pulse was 50 μs. The final value of t_2 was 51.2 ms and an additional 250 ms was inserted at the end of every t_2 period. Since eight 32-step phase cycles were employed, the total time was 2.89 h. (b) A contour plot of the spectrum in part a. (c) The projection of the spectrum in part a onto the ν_2 axis. The parameters for the simulation (dashed line above, solid lines below) shown in the inset are given in the text. (d) The projection of the spectrum in part a onto the ν_1 axis. The parameter for the simulation (dashed line above, solid line below) shown in the inset is given in the text.

inhomogeneities, does, again, decrease the accuracy of this value. Also, the t_1 noise (evident in Figure 5a) probably makes a significant contribution to the mismatch of the simulation at the base of the peak (inset of Figure 5d).

Discussion

Pekar and Leigh have discussed the advantages of Fourier transforming the 2Q-filtered 1Q time domain signal (Figure 2a, eq 6) obtained with fixed values of the 2Q creation time, τ, and evolution time, t_1.[9] Although this experiment edits type d contributions from the ^{23}Na spectrum[10] and inverts the phases of the 1Q satellite (12, 34) transitions (thus making them easier to detect), it actually decreases the relative intensity of the latter (from 60% to 50%). In addition, it still suffers from receiver dead time problems and if the 1Q satellite signals are NMR invisible for this reason, they still will be after 2Q filtering (eq 9).[11] In this paper, we have presented some results of the more diagnostic, though also more time-consuming, full 2D (t_1 incrementation) experiment.

The correlation map seen for the 2D2Q spectrum of the oriented liquid crystalline sample in Figure 3b exhibits a particularly interesting feature. Although both of the 2Q lines correlate with the 1Q central line (23, Figure 1) they each correlate with different 1Q satellite lines. The high-fequency 2Q line (24) correlates with only the high-frequency 1Q satellite line (34) and the low-frequency 2Q line (13) correlates with only the low-frequency 1Q satellite line (12). This can be qualitatively understood by visualizing each 2QC as excited by a two-photon process where the photons are resonant with the appropriate energy levels as unperturbed by a radiation field (Figure 1, right). This results in the fact that the splitting of the 2Q doublet, 33.8 kHz (Figure 3d), equals the splitting of the 1Q satellite lines (figure 3c). This is in contrast to a high-power CW experiment, which can be viewed as involving a two isochromatic, nonresonant photon process, and which produces a 2Q doublet splitting of one-half that of the 1Q satellites. This has been reported for the ^{23}Na spectrum of a type b sample.[34] (In the paper describing this experiment,[34] the left-hand sides of eq 2 should be divided by 2, 2, and 3.)

It is very important that both of the 2Q lines correlate with the 1Q central line because this means that all of the 2Q spectral information can derive from the sharp, always observable, 1Q central line. This is particularly evident in the 2D2Q powder pattern spectrum (Figure 4). The powder pattern nature of the 1Q spectrum can be hard to detect (Figure 4c, nonexpanded). This would be especially true if the spectrum exhibited a more common signal-to-noise ratio (much poorer than that of Figure 4c) or consisted of a superposition of several powder patterns of different breadths and extents of homogeneous broadening (a possibility, for biological tissue). However, the powder pattern nature of the

(34) Lindblom, G.; Wennerström, H.; Lindman, B. *J. Magn. Reson.* **1976**, *23*, 177–179.

2Q spectrum (Figure 4e) is hard to miss. There is no sharp central line to obscure the inhomogeneously broadened satellite transitions.

The 2D2Q experiment is also informative in the homogeneous biexponential case (Figure 5). Although not the situation here, it is possible that the broad 1Q component (12, 34, Figure 1) is so broad as to be undetectable in simple pulse experiments because the receiver dead time cannot be made short enough (again, a possibility for biological tissue; see, for example, ref 35). However, very broad 2Q resonances can always be observed because there is no significant dead time in the t_1 time domain.

As we saw in the Theory section, the order of increasing line width would be 1Q central line, 2Q line, and 1Q satellite line in the type c case if random motion characterized by a single value of τ_c obtained. This is not the case in the projections of Figure 5. The apparent 2Q line width (247 Hz) is greater than the 1Q satellite line width (124 Hz). However, because of the poor digital resolution in ν_1 (DR(ν_1) = 78 Hz) and the greater sensitivity to field inhomogeneities, it is not possible to be absolutely sure whether the 2Q line has a greater natural line width than that of the broad 1Q line. If it did, that would be consistent with the expectation that the decription of the motion of the EFG magnitude-orientation product in these systems requires at least two long correlation times.

Probably the most useful aspect of the 2D2Q experiment, however, is the ability of the 2Q dimension to identify the cause of NMR invisibility in the 1Q dimension. The two mechanistic extremes of this phenomenon are the inhomogeneous powder pattern (Figure 4c) and homogeneous biexponential relaxation (Figure 5c). If the broad components are truly undetectable, one cannot ascertain the details from the 1Q spectrum. However, the 2Q spectrum is always detectable (since its features derive from the 1Q central line and it has no dead time problems) and the two mechanistic extremes (Figures 4e and 5d) are easily distinguishable.

With real biological samples, it is quite possible to have a coexistence or superposition of type b and type c spectra and/or spectra of intermediate natures (exchange). Figure 2b is an attempt to give an idea of the situation with regard to simultaneously exciting 2QC from each of these mechanistically extreme spectra. The excitation function $A(\bar{\omega}_Q,\tau)$ (eq 3) is plotted as a function of τ for the particular case when $\bar{\omega}_Q/2\pi$ = 1 kHz (a small value). The decay as a function of τ arises because the 2nd and 3rd rank 1Q coherences were assigned R values of 10^3 s^{-1} each. Larger values of $\bar{\omega}_Q$ would "pile up" the A curve at shorter values of τ. A similar kind of thing happens with $f(\alpha,\tau)$ (eq 8), which is shown for the particular case when R_s^{1Q} = 100 s^{-1} and α = 20. Larger values of α cause this function to become greater and to peak at shorter values of τ. A sample giving rise to a superposition of spectra may have several (or even a distribution of) values of $\bar{\omega}_Q$ and/or α which are weighted by the fraction of nuclei in these different environments. Thus, the 2QC of these environments will be excited with different efficiencies. The degree to which the 2Q spectrum (ν_1) can detect the different environments depends on the excitation efficiency. Although this could be viewed as a problem, it may actually be an advantage because the extent of resolution of spectral components in ν_1 depends on DR(ν_1) and field inhomogeneity. As we have said before, decreasing DR(ν_1) (increasing the resolution) requires lengthening the total time of the experiment (eq 14). Thus, the ability to separately excite spectral components tending toward the type b and type c extremes could prove to be very useful.

We have recently also observed the 2D2Q ^{35}Cl (I = $^3/_2$) spectra of model systems.[36]

Acknowledgment. We thank Jim Pekar and Ronald Summers, Dr. Jim Balschi, and Professors Gerry Harbison, Phil Johnson, Jack Leigh, Bob Lenkinski, Harold Friedman, Peter Joseph, and Bob Griffin for stimulating discussions. Marie Dippolito for typing the manuscript, and the National Science Foundation (Grant No. PCM 84-08339) and the National Institutes of Health (Grant No. GM 32125) for support of this work.

Registry No. Sodium dodecylsulfate, 151-21-3; *n*-decyl alcohol, 112-30-1.

(35) Rooney, W. D.; Barbara, T. M.; Springer, C. S., manuscript in preparation.

(36) Xu, Y.; Springer, C. S., manuscript in preparation.